# Numerical Implementations of PML Boundary Conditions in the TLM-Based SCN FDTD Grid

Jian Xu, Zhizhang Chen, and Jimmy Chuang

***Abstract*— The recently developed perfectly matched layer (PML) absorbing scheme and its improvement, the modified PML (MPML), have been shown to be very effective in absorbing numerical electromagnetic (EM) waves in the conventional finite-difference time-domain (FDTD) method. However, the implementation of PML in the transmission-line-matrix (TLM) method is not straightforward. An alternative and easy way is to use the recently introduced TLM-based symmetrical condensed node (SCN) FDTD method. In this paper, the implementation of the PML and MPML schemes in the TLM-based SCN FDTD method and the extension of the MPML to three dimensions are presented. The computation amount is found to increase by a maximum of 1/3, and the MPML is shown to be effective and efficient in absorbing both the evanescent and propagating modes.**

***Index Terms*— Absorption, TLM-based finite-difference time-domain (FDTD), perfectly matched layer (PML).**

## I. Introduction

Since the finite-difference time-domain (FDTD) method was introduced in 1966 [1], different forms of the FDTD method have been developed. One of the recently developed FDTD schemes is the generalized TLM-based SCN FDTD method, which can be equivalent to the three-dimensional (3-D)-transmission-line-matrix (TLM) symmetrical condensed node (SCN) model [2]–[4] (the method was then called the TLM-based FDTD). The main feature of the method is that it is still a TLM-based technique, but formulated in an FDTD fashion. As a result, it allows direct use of field quantities and direct incorporation of full anisotropic media, while retaining certain features of both the FDTD and TLM methods.

Like many other numerical techniques, in order to simulate infinite space relevant to open structures, the FDTD methods need so-called absorbing boundary conditions (ABC's) to truncate an infinite problem space to a finite computation domain without incurring very large errors. Recently, an absorbing condition, the perfectly matched layer (PML) ABC's, was proposed [5]. By splitting Maxwell's equations and introducing both the electric and magnetic losses, multiple anisotropic lossy layers have been constructed in such a way that the intrinsic impedances between the layers are matched while waves are attenuated as they propagate in the lossy PML media. Theoretically, as well as experimentally, PML is found to be able to effectively absorb both propagating and evanescent regardless of the incident angles and frequencies [6], [7]. The further enhancement of the PML's ability in absorbing nonpropagating waves without affecting the absorption for the propagating waves has lead to a modified perfectly matched layer (MPML) for FDTD meshes in the two-dimensional (2-D) case [8]. Preliminary results have demonstrated that the MPML has a very good absorption of numerical waves in the conventional 2-D FDTD grids of Yee's scheme.

The TLM method is another powerful time-domain numerical method introduced by Johns [9] for solving electromagnetic (EM) problems [10], [11]. In principle, the TLM is based on the analogy between the EM fields and voltage/currents in a mesh of interconnected transmission lines. Therefore, all the field quantities to be simulated have to be converted to the corresponding circuit parameters in terms of voltage impulses. Although the conversion is not complicated most of the times, it does pose certain difficulties or becomes complicated in certain cases, e.g., simulation of nonlinear media. In the case of implementation of the PML, the difficulty arises in how to realize the split Maxwell's equations in a TLM mesh. However, a recently proposed FDTD method—the generalized TLM-based SCN FDTD method as mentioned earlier, can circumvent this problem. In this paper, the implementation of PML and MPML schemes in the TLM-based SCN FDTD method, is described and numerical experiments are performed. The results demonstrate the effectiveness and efficiency of the MPML in the TLM-based SCN FDTD grid. In addition, the extension of the MPML to three dimensions is derived.

In the Section II, the TLM-based SCN FDTD scheme is briefly outlined. In Section III, the extension of MPML formulations to three dimensions is described. In Section IV, the implementation of the PML in the TLM-based SCN FDTD is detailed, while in Section V, the numerical test results are demonstrated. Finally, in Section VI, conclusions and a summary are presented.

## II. The TLM-Based SCN FDTD

The details of the TLM-based SCN method is described in [4]. A brief description of the method is provided in the following paragraphs.

In the new TLM-based SCN FDTD scheme, all the electric and magnetic quantities are defined at the center of a cell while the tangential electric and magnetic fields are defined at the boundary surfaces of the cell (Fig. 1). As a result, the continuities of the tangential electric and magnetic fields across the interface of two neighboring cells are automatically ensured. For a dielectric interface, no additional conditions, such as the one used in [12], for the conventional FDTD method need to be introduced. The field continuities are inherent in the TLM-based SCN FDTD algorithm.

### A. Update of Field Quantities at the Center of the 3-D Cell

With the new grid arrangements as shown in Fig. 1, the field values at the center of a 3-D cell can be updated by directly finite-differencing Maxwell's equations. For example,

$$\begin{aligned}\frac{D_x^n(i,j,k)-D_x^{n-1}(i,j,k)}{\delta t} &= -\sigma_x\frac{E_x^n(i,j,k)+E_x^{n-1}(i,j,k)}{2}\\ &\quad+\frac{H_z^{n-\frac{1}{2}}\left(i,j+\frac{1}{2},k\right)-H_z^{n-\frac{1}{2}}\left(i,j-\frac{1}{2},k\right)}{\delta y}\\ &\quad-\frac{H_y^{n-\frac{1}{2}}\left(i,j,k+\frac{1}{2}\right)-H_y^{n-\frac{1}{2}}\left(i,j,k-\frac{1}{2}\right)}{\delta z}.\end{aligned}\tag{1}$$

Here, $E^{n-\frac{1}{2}}$ is approximated with $(E^n+E^{n-1})/2$. $\delta y$ and $\delta z$ are the space increments in the $y$- and $z$-direction, respectively. $\sigma_x$ is the electric conductivity in the $x$-direction. The equations for the other components can be obtained in a similar way or by permutating the indexes.

From the above equations, the field quantities at the center of a 3-D cell can be found if the constitutive relationships of a medium, $\boldsymbol{D}=\boldsymbol{D}(\boldsymbol{E})$ and $\boldsymbol{B}=\boldsymbol{B}(\boldsymbol{H})$, are known.

Manuscript received June 11, 1996; revised February 26, 1997. This paper was supported by the Natural Science and Engineering Research Council of Canada.

J. Xu and Z. Chen are with the Department of Electrical Engineering, Technical University of Nova Scotia, Halifax, N.S., Canada B3J 2X4.

J. Chuang is with the Department of Mechanical Engineering, Technical University of Nova Scotia, Halifax, N.S., Canada B3J 2X4.

Publisher Item Identifier S 0018-9480(97)05385-4.

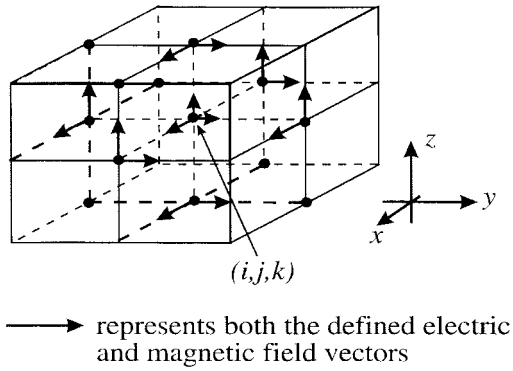


Fig. 1. Grid arrangement for the TLM-based FDTD scheme.

### *B. Update of the Field Components at the Boundary Surfaces*

For the field values at the boundary surfaces, a special averaging process can be applied. For instance, at the boundary surface $\left(i,\, j,\, k+\frac{1}{2}\right)$ one can have

$$\begin{aligned}
&\delta x E_x^{n+\frac{1}{2}}\left(i,\, j,\, k+\frac{1}{2}\right)\\
&\quad=\frac{\delta x E_x^{n-\frac{1}{2}}\left(i,\, j,\, k-\frac{1}{2}\right)+\eta\delta y H_y^{n-\frac{1}{2}}\left(i,\, j,\, k-\frac{1}{2}\right)}{2}\\
&\qquad+\frac{\delta x E_x^{n-\frac{1}{2}}\left(i,\, j,\, k+\frac{3}{2}\right)-\eta\delta y H_y^{n-\frac{1}{2}}\left(i,\, j,\, k+\frac{3}{2}\right)}{2}\\
&\qquad+\left[\delta x E_x^{n}(i,\, j,\, k)+\eta\delta y H_y^{n}(i,\, j,\, k)\right]\\
&\qquad+\left[\delta x E_x^{n}(i,\, j,\, k+1)-\eta\delta y H_y^{n}(i,\, j,\, k+1)\right] \qquad (2a)\\
&\eta\delta y H_y^{n+\frac{1}{2}}\left(i,\, j,\, k+\frac{1}{2}\right)\\
&\quad=\frac{\delta x E_x^{n-\frac{1}{2}}\left(i,\, j,\, k-\frac{1}{2}\right)+\eta\delta y H_y^{n-\frac{1}{2}}\left(i,\, j,\, k-\frac{1}{2}\right)}{2}\\
&\qquad-\frac{\delta x E_x^{n-\frac{1}{2}}\left(i,\, j,\, k+\frac{3}{2}\right)-\eta\delta y H_y^{n-\frac{1}{2}}\left(i,\, j,\, k+\frac{3}{2}\right)}{2}\\
&\qquad+\left[\delta x E_x^{n}(i,\, j,\, k)+\eta\delta y H_y^{n}(i,\, j,\, k)\right]\\
&\qquad-\left[\delta x E_x^{n}(i,\, j,\, k+1)-\eta\delta y H_y^{n}(i,\, j,\, k+1)\right] \qquad (2b)
\end{aligned}$$

where $\eta=\sqrt{\frac{\mu_0}{\varepsilon_0}}$ can be chosen as the free-space intrinsic impedance.

Note the above formulas resulting from the averaging process do not change with the constitutive parameters, but remain the same for anisotropic and nonlinear materials. In addition, it is noted that the above averaging scheme has also been obtained by a process involving *characteristic decomposition* of EM fields [13].

The equations for other components at the other boundary surface of a 3-D cell can be obtained in a similar form or by permutating the indexes.

## III. MPML in Three Dimensions

PML's consists of multiple anisotropic layers with both electric and magnetic losses, leading to the attenuation of a wave. A perfect absorption can then, in theory, be obtained regardless of frequency and incident angles. With the careful selection of electric- and magnetic-loss spatial profiles and the careful implementation of the PML scheme into a numerical grid, a high absorption has been obtained experimentally for the conventional FDTD method [5], [6].

The further enhancement of the absorption of the evanescent modes with the PML has led to the development of the MPML scheme in two dimensions [8]. The main component of the MPML is the introduction of the extra degrees of freedoms, so that the absorption of evanescent energy can be controlled with these freedoms. The numerical results have proven the effectiveness of the MPML in two dimensions. The MPML was shown being placed in closer proximity to the scatterers than the normal PML [8]. Again, careful selections of spatial loss profiles are required in order to reduce reflections caused by numerical dispersion.

To allow the computation of more realistic 3-D structures, MPML formulations are extended to three dimensions in the following paragraphs.

As was performed for the normal PML, Maxwell's equations can be divided into 12 equations. For example, one can have

$$\mu_0\mu_y\frac{\partial H_{xy}}{\partial t}+\sigma_y^* H_{xy}=-\frac{\partial E_z}{\partial y} \qquad (3a)$$

$$\mu_0\mu_z\frac{\partial H_{xz}}{\partial t}+\sigma_z^* H_{xz}=\frac{\partial E_y}{\partial z} \qquad (3b)$$

$$\epsilon_0\epsilon_y\frac{\partial E_{xy}}{\partial t}+\sigma_y E_{xy}=\frac{\partial H_z}{\partial y} \qquad (4a)$$

$$\epsilon_0\epsilon_z\frac{\partial E_{xz}}{\partial t}+\sigma_z E_{xz}=-\frac{\partial H_y}{\partial z}. \qquad (4b)$$

The other split equations can be obtained in a similar way.

Note here that in addition to the normal quantities $\sigma_x$, $\sigma_y$, $\sigma_z$, $\sigma_x^*$, $\sigma_y^*$, and $\sigma_z^*$, extra quantities $\epsilon_x$, $\epsilon_y$, $\epsilon_z$, $\mu_x$, $\mu_y$, and $\mu_z$ are introduced in the split equations in order to control the absorption of evanescent energy. By following the procedure similar to that for two dimensions [8], the match conditions can be derived as follows:

$$\frac{\sigma_x}{\epsilon_0}=\frac{\sigma_x^*}{\mu_0},\ \frac{\sigma_x}{\epsilon_0}=\frac{\sigma_x^*}{\mu_0},\ \frac{\sigma_x}{\epsilon_0}=\frac{\sigma_x^*}{\mu_0} \qquad (5a)$$

$$\epsilon_x=\mu_x,\ \epsilon_y=\mu_y,\ \epsilon_z=\mu_z. \qquad (5b)$$

In other words, when the above conditions are satisfied, theoretically, the reflections between two neighboring MPML layers are zero, regardless of incident angles and frequencies. In order to achieve the minimum numerical reflections, the electric losses and the permittivities need to be carefully chosen. For example, considering the MPML layers, as shown in Fig. 2, one can use

$$\begin{aligned}
\sigma_z&=\sigma_z^{\max}\left(\frac{\rho}{\delta}\right)^2\\
\epsilon_z&=1+\epsilon_z^{\max}\left(\frac{\rho}{\delta}\right)^2
\end{aligned} \qquad (6)$$

where $\delta$ is the MPML thickness, $\sigma_z^{\max}$ is the maximum conductivity which the PML can arise to, and $(\epsilon_z^{\max}+1)$ is the maximum permittivity.

With the above conditions, if the MPML is terminated with a conducting wall, the MPML reflection coefficient can be found as follows:

$$R_z(\theta)=e^{-2\sigma_z^{\max}\sigma\cos(\theta)/(n+1)\epsilon_0 c}, \qquad \text{for propagating modes} \qquad (7)$$

$$R_{zen}=e^{-2\epsilon_z k\sinh(\alpha)z}, \qquad \text{for evescent modes} \qquad (8)$$

where $c$ is the speed of light, $k=\omega/c$, and $\alpha$ is a real number and larger than zero.

Equation (7) is the same as that for the PML. This means that the introduction of extra freedoms does not change the absorbing performance for propagating modes. However, as can be seen from (8), the additional parameters, $\epsilon_z$ (and $\mu_z$) increase the degree of absorption of evanescent modes.

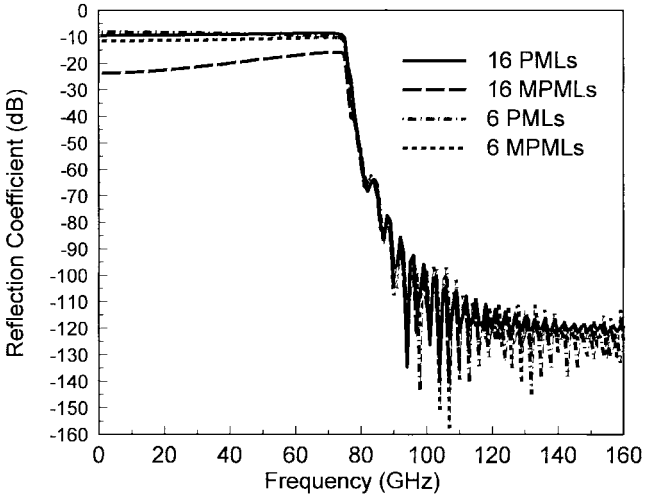


Fig. 2. Return loss of $TE_{31}$ mode in the WR28 waveguide with both ends terminated with PML's. The cutoff frequency is 76 GHz.

## IV. Implementations of MPML to the TLM-Based SCN FDTD

The implementation is rather straightforward. The reason is that in the TLM-based SCN FDTD grids, all six field components are defined at the center of the 3-D cell, and Maxwell's equations are only applied in respect to the center of a cell. Consequently, only the field components at the center of a 3-D cell need to be split, while the field components at the boundary surfaces are not. They are still computed via the averaging procedure involving the total fields at the center of a 3-D cell. The averaging process is not affected by the split of field components in the PML regions. In comparison with the original computation, computation expenditure is only increased by a maximum of 1/3.

By differencing (3a), (3b) and (4a), (4b), the MPML formulations can easily be implemented in the TLM-based SCN FDTD. For example, considering (3b), one has

$$\mu_0\mu_z(i,j,k)\frac{H_{xz}^n(i,j,k)-H_{xz}^{n-1}(,j,k)}{\delta t} + \sigma_z^*(i,j,k)\frac{H_{xz}^n(i,j,k)+H_{xz}^{n-1}(i,j,k)}{2} = \frac{E_y^{n-\frac{1}{2}}\left(i,j,k+\frac{1}{2}\right)-E_y^{n-\frac{1}{2}}\left(i,j,k-\frac{1}{2}\right)}{\delta z} \quad (9)$$

which can be rewritten as

$$\eta H_{xz}^n(i,j,k) = C_{xz}(i,j,k)\left[D_{xz}(i,j,k)\eta H_{xz}^{n-1}(i,j,k) + \frac{E_y^{n-\frac{1}{2}}\left(i,j,k+\frac{1}{2}\right)-E_y^{n-\frac{1}{2}}\left(i,j,k-\frac{1}{2}\right)}{\delta z}\right] \quad (10)$$

with

$$C_{xz}(i,j,k)=\left\{\sqrt{\frac{\epsilon_0}{\mu_0}}\left[\frac{\mu_z(i,j,k)}{\delta t}+\frac{\sigma_z^*(i,j,k)}{2}\right]\right\}^{-1} \quad (11)$$

$$D_{xz}(i,j,k)=\left\{\sqrt{\frac{\epsilon_0}{\mu_0}}\left[\frac{\mu_z(i,j,k)}{\delta t}-\frac{\sigma_z^*(i,j,k)}{2}\right]\right\}^{-1}. \quad (12)$$

As seen, the field values at the cell center in a PML region can be obtained from the values of $H$-field and the $E$-field at the boundary surfaces and at the previous time step. Since the field components at the boundary surface are not split in a TLM-based SCN FDTD grid, the only work in the implementation of the PML is to separately compute $H_{xz}$ and $H_{xy}$ at the center of a cell [as indicated by (9)] and then sum them together to get the total $H_z$. Therefore, implementation of the PML (or MPML) in the TLM-based SCN FDTD grid is relatively easy and convenient.

The PML equations for other components can be similarly constructed. Again, the process is straightforward.

Unlike the PML implementation so far in the conventional FDTD grid where the last layer of a PML region is terminated with a conducting wall (causing a total reflection at the end of a PML region), a zero reflection coefficient (i.e., $E/H$ = free-space impedance) is terminated in the PML region in the TLM-based SCN FDTD grid. It is equivalent to terminating a PML region with a damping load, resulting in a further dissipation of the energy in PML region. A better absorption is then expected here, as opposed to terminating with a conducting wall. As to the implementation of this zero reflection coefficient in the TLM-based SCN FDTD scheme, it is straightforward, since both the electric and magnetic fields are defined at the boundary surfaces of a 3-D cell.

## V. Numerical Results

Several cases are tested to ascertain the accuracy levels which are associated with the PML in the TLM-based SCN FDTD grid. These cases are: 1) a plane wave normally incident on the PML; 2) wave propagation in a rectangular waveguide with both ends terminated with PML's; and 3) wave propagation in a microstrip line with the open space simulated with the PML.

### *Case A: A Plane Wave Normally Incident onto a PML*

A plane-wave propagation is the simplest wave one can use to test the absorbing performance of an absorbing condition. Like the 3-D TLM symmetrical condensed node, the TLM-based SCN FDTD shows no numerical dispersion in its axial direction in the free space. Therefore, if a plane wave is launched along one of its axial directions, no dispersion should be observed. When a PML region is terminated, experiments show that the numerical reflection is completely zero. In other words, PML or MPML have a perfect absorption of a plane wave. Further studies indicate that this perfect absorption does not changes with different loss profiles. This is due to the fact that the plane wave, which is attenuated along its way toward the end of a PML region, is finally absorbed by the zero reflection wall placed at the end of the PML region. Although one may then argue about the effectiveness of the PML, the PML does not produce numerical reflections. In this sense, the properties of a discrete PML are in good match with those of the TLM-based SCN FDTD grid.

### *Case B: A Dominant $TE_{10}$ Mode in a Rectangular Waveguide*

The second example for testing is a section of a WR28 waveguide with both ends terminated with PML and MPML layers. The rectangular waveguide is chosen because waves inside the guide can be considered as the superposition of many plane waves with different incident angles, which are associated with the operating frequencies. In addition, evanescent modes can be clearly identified by selecting the operating frequency points below the cutoff frequencies. All of this allows one to numerically evaluate the overall performance of the PML in the TLM-based SCN FDTD grid.

The waveguide, which has a dimension of $7.112 \times 3.556$ mm$^2$, is discretized into 28 $\Delta l$ in width, 14 $\Delta l$ in height, and 100 $\Delta l$ in length ($\delta x = \delta y = \delta z = \Delta l$ is chosen in this case). Six and 16 MPML and PML layers were placed at both ends of the waveguide, respectively. The maximum electric loss was chosen as 1.24 for the

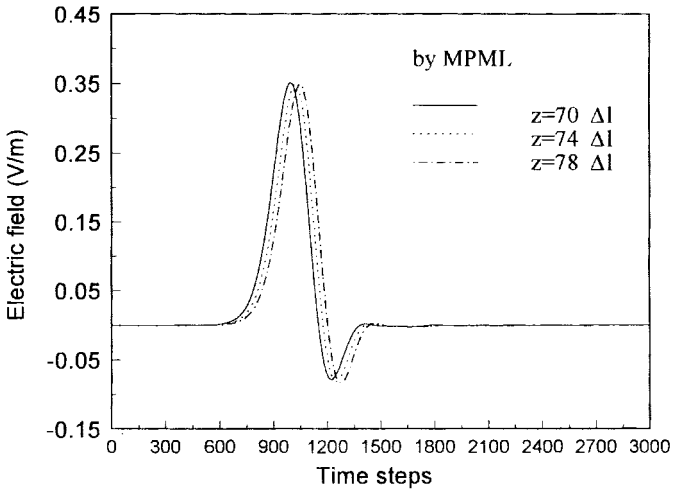


Fig. 3. The electric fields at three different locations in the microstrip line boxed by the MPML.

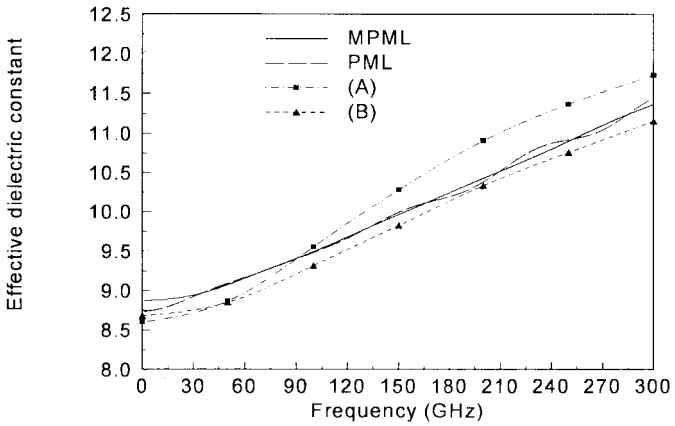


Fig. 4. Comparison of the effective dielectric constant as computed with different methods. (a) Edward and Owen [14]. (b) Zhang *et al.* [12].

reflection coefficient equal to $10^{-6}$. The maximum dielectric constant of the MPML was chosen as five.

Fig. 2 shows the return loss of the waveguide for the $TE_{31}$ mode. As can be seen, the return loss is below $-80$ dB for propagation modes with both six and 16 PML or MPML layers. For the evanescent modes, a better absorption for 16 MPML layers is achieved.

### *Case C: Wave Propagation in Microstrip Lines*

Consider a microstrip structure which is boxed by PML layers. The parameters used in computation are the same as those used in [12]. A uniform excitation was imposed under the microstrip, and waves were measured at two locations just below the microstrip. The computation box is 22 $\Delta l$ $\times$ 40 $\Delta l$ $\times$ 100 $\Delta l$, which includes ten MPML layers in all three directions.

Fig. 3 shows the recorded time variations of the vertical electric field under the microstrip at different positions along the propagation direction ($z$ = direction). Fig. 3 is the result calculated with MPML. Fig. 4 shows the comparison of the effective dielectric constant calculated with the PML, MPML, and other methods. It is obvious that the curve representing the results with the MPML is smooth (and, therefore, more accurate), while the curve for the PML shows some degree of oscillation. The reason is that the MPML is more effective in absorbing the evanescent energy as explained earlier and shown in the waveguide case. In general, the MPML and PML results agree well. However, both of them are a bit lower than the result obtained with the empirical model [14], but higher than the values presented in [12] with the conventional FDTD method (which uses a simple absorbing condition). Therefore, one can say that the TLM-based SCN FDTD method with the MPML does present accurate solutions to inhomogeneous structures.

## VI. Conclusions

In this paper, the extension of the MPML to three dimensions, and the implementation of the MPML in the TLM-based SCN FDTD method have been presented. It is found that the implementation of the PML or MPML in the TLM-based SCN FDTD grid is relatively easy and straightforward, and the computation expenditures for PML calculations are only increased by a maximum of 1/3. This is attributed to the capability of the TLM-based SCN FDTD method in defining all the field components at grid points, and in easy treatments of the anisotropic media, as pointed out in [3]. In addition, due to the fact that both electric and magnetic fields are defined at grid points, additional treatments at the dielectric-air interface are not required. In conclusion, the PML and MPML have been implemented in the TLM-based SCN FDTD scheme and have been shown to be effective in absorbing both propagating and evanescent energy. Numerical results are in good agreement with either theoretical predictions or with results obtained from other techniques.

Finally, it is worth mentioning that unsplit PML formulations have been recently proposed [15]. They have been shown as effective as the original PML while saving memory and control processing unit (CPU) time. The implementation of the unsplit PML schemes in the TLM-based FDTD method should be both straightforward and easy. However, the main objective of this paper is to numerically validate the applicability and effectiveness of the PML scheme in the TLM-based SCN FDTD grid.

## Acknowledgment

The authors wish to thank the reviewers for their useful comments and suggestions.

## References

[1] K. S. Yee, "Numerical solution of initial boundary value problems involving Maxwell's equations in isotropic media," *IEEE Trans. Antennas Propagat.*, vol. AP-14, pp. 302–307, May 1966.

[2] Z. Chen, M. M. Ney, and W. J. R. Hoefer, "A new finite-difference time-domain formulation and its equivalence with the TLM symmetrical condensed node," *IEEE Trans. Microwave Theory Tech.*, vol. 39, pp. 2160–2169, Dec. 1991.

[3] Z. Chen, "The generalized TLM-based SCN finite-difference time-domain method and its applications to frequency-dependent and anisotropic media," *IEEE Int. Microwave Symp. Dig.*, San Francisco, CA, June 16–21, 1996, pp. 435–438.

[4] Z. Chen and X. Xu, "The generalized TLM based finite-different time-domain method and its applications to frequency-dependent and anisotropic media," *IEEE Trans. Microwave Theory Tech.*, to be published.

[5] J. P. Berenger, "A perfectly matched layer for the absorption of electromagnetic waves," *J. Comput. Phys.*, pp. 185–200, Oct. 1994.

[6] D. S. Katz, E. T. Thiele, and A. Taflove, "Validation and extension to three dimensional of the Berenger PML absorbing boundary condition for FD-TD meshes." *IEEE Microwave Guided Wave Lett.*, vol. 4, pp. 268–270, Aug. 1994.

[7] Z. Wu and J. Fang, "Numerical implementation and performance of perfectly matched layer boundary conditions for waveguide structures," *IEEE Trans. Microwave Theory Tech.* vol. 43, pp. 2676–2683, Dec. 1995.

[8] B. Chen, D. G. Fang, and B. H. Zhou, "Modified Berenger PML absorbing boundary condition for FD-TD meshes," *IEEE Microwave Guided Wave Lett.*, vol. 5, pp. 399–401, Nov. 1995.

[9] P. B. Johns, "A symmetrical condensed node for the TLM method," *IEEE Trans. Microwave Theory Tech.*, vol. MTT-35, pp. 270–377, Apr. 1987.
[10] W. J. R. Hoefer, "The transmission line matrix method," in *Numerical Techniques for Microwave and Millimeter Wave Passive Structures*, T. Itoh, Ed. New York: Wiley, 1989, pp. 496–591, ch. 8.
[11] C. Christopoulos, *The Transmission Line Modeling Method (TLM)*. Piscataway, NJ: IEEE Press, 1995.
[12] X. Zhang, J. Fang, and K. K. Mei, "Calculations of the dispersive characteristics of microstrips by the time-domain finite-difference method," *IEEE Trans. Microwave Theory Tech.*, vol. 36, pp. 263–267, Feb. 1988.
[13] J. LoVetri and N. R. S. Simons, "A class of symmetrical condensed node TLM methods derived directly from Maxwell's equations," *IEEE Trans. Microwave Theory Tech.*, vol. 41, pp. 1419–1428, Aug. 1993.
[14] K. C. Gupta, R. Grag, and R. Chadha, *Computer-aided Design of Microwave Circuits*. Norwood, MA: Artech House, 1981.
[15] L. Zhao and A. C. Cangellaris, "A general approach for the development of unsplit-field time-domain implementations of perfectly matched layers for FDTD grid truncation," *IEEE Microwave Guided Waves Lett.*, vol. 6, pp. 209–211, May 1996.

# Hybrid FDTD Large-Signal Modeling of Three-Terminal Active Devices

Qiang Chen and V. F. Fusco

***Abstract*—A general algorithm for including large-signal active three-terminal models into the finite-difference time-domain (FDTD) method is presented. A dynamic interface between the active device and the FDTD lattice is used to simulate the prominent nonlinear time-dependant behavior of the three-terminal active device, which is connected across multiple FDTD cells. A technique for introducing an internal electromagnetic (EM) field absorber into the FDTD three-terminal active device model in order to eliminate undesired current coupling is discussed. Numerical comparison shows this method is accurate and expected to have general utility for other complicated hybrid lumped-circuit FDTD modeling situations.**

***Index Terms*— Active devices, finite-difference time-domain method, large-signal models.**

## I. Introduction

Lumped-element modeling is a very important aspect for the future development and application of the finite-difference time-domain (FDTD) method [1]–[7]. It is well accepted that a lumped element can be represented by lumped-current(s) in the FDTD algorithm. To accurately represent a general lumped-element case, this lumped-current should satisfy two requirements.

1) It should be connected across multiple, rather than (as at present) single, FDTD cells so that an arbitrarily sized lumped element can be modeled.
2) A dynamic interface between the FDTD electromagnetic (EM) fields and the lumped element's *I–V* behavior (i.e., the lumped-current) should be calculated using the present, rather than the former, time-step of the discretized EM field in such a way that the obtained lumped-current is correct for both the FDTD EM-field computation and the lumped-element *I–V* characteristic at any given time-step.

Manuscript received May 1, 1996; revised February 26, 1997. This work was supported by the United Kingdom Engineering and Physical Science Research Council Grant GR/J40188.

The authors are with the High-Frequency Electronics Laboratory, Department of Electrical and Electronic Engineering, The Queen's University of Belfast, Belfast BT9 5AH, Northern Ireland.

Publisher Item Identifier S 0018-9480(97)05386-6.

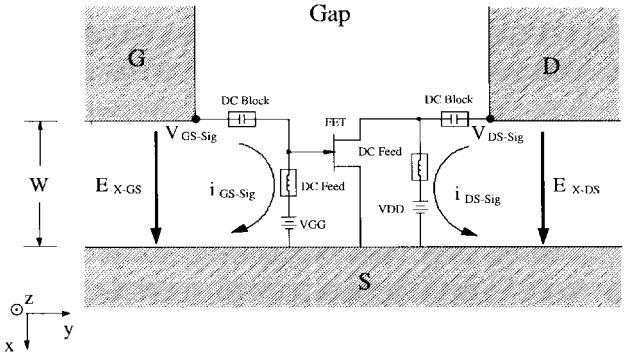


Fig. 1. Interface region between FDTD solver field and three-terminal device model.

The first above-mentioned requirement was recently addressed by Durney *et al.* [5] and the second by Piket-May *et al.* [6], where a semi-implicit average of present and former time-step values was used. However, due to numerical complexities involved, these two aspects have not been accounted for concurrently. The parametric technique [7] is an attempt to take these two requirements simultaneously into account. The technique is simple and accurate for simple lumped-elements, i.e., a resistor, a capacitor, a diode, etc. However, for complicated lumped-element circuits, it is difficult to simulate their behavior by the method of media parameters variation. In this paper, an FET connected across a unilaterally gapped slotline (Fig. 1) is taken as an example of a general method for lumped-element modeling. Since the FET large-signal model is indeed a complex three-terminal nonlinear lumped-element circuit containing passive, source, and control elements, the method presented here is expected to be useful for any other lumped-element/circuit models. In addition, in this paper, the decoupling between the lumped gate current and lumped drain current in the FET FDTD model is discussed.

## II. Interface Between Slotline Field and FET Model

Table I shows the parameters of a general packaged large-signal FET model,[1] [8] customized for the NE72089 device to be included into the FDTD algorithm. Its nonlinear port (source and drain) currents can be calculated by time-domain analysis by solving a set of differential equations provided the port voltages are known. Thus, the obtained lumped currents are then used in the FDTD algorithm for the interaction of FDTD EM fields and the FET behavior. Fig. 1 shows the port voltages and port currents as an interface between the distributed fields and the FET model in the slotline example. The unilateral slotline gap between the source and drain of the FET is for dc bias. From the figure, it can be seen that dc-bias voltages are applied and simulated directly in the FET model. Thus, only signal fields (with no dc bias) are analyzed by the FDTD method in the slotline. This simplifies the FDTD simulation and gives an advantage for any further circuit simulation using the hybrid field. For the simulation of other circuits with a high level

[1] HP 85150B Microwave and RF Design Systems, *Microwave Library Components (Lumped, Ideal, & Nonlinear)*, ch. 17, vol. 4, Component Catalog, Hewlett-Packard Company, 1994.